# Determination of the magnitude and sign of the $^{185,187}$Re nuclear electric quadrupole coupling constants using nuclear acoustic resonance

R. K. Sundfors
*Ultrasonics Laboratory, Department of Physics, Washington University, St. Louis, Missouri 63130*
(Received 9 November 1989)

Acoustic nuclear electric quadrupole resonance spectra and the magnitude and sign of the coupling constants for $^{185}$Re and $^{187}$Re in rhenium-metal single crystals have been measured using nuclear acoustic resonance (NAR) in a small magnetic field. These measurements were carried out using a NAR reflection bridge spectrometer in the 37–41 MHz frequency range and at 4.2 and 77.8 K. In this hexagonal crystal, the dynamic coupling between acoustic waves and the Re nuclear spin systems is shown to be via the dynamic quadrupole interaction, which is responsible for the observation of both $\Delta m = \pm 1$ and $\pm 2$ transitions between the $\pm\frac{3}{2}$ energy levels and the mixed $\pm\frac{1}{2}$ energy levels. Magnetic-resonance second moments for angular-independent indirect exchange broadening and angular-dependent static electric quadrupole broadening (from a spread in the electric quadrupole coupling constant value) are determined from the measured linewidths.

## I. INTRODUCTION

The nuclear magnetic resonance of $^{185}$Re and $^{187}$Re in rhenium metal has only been observed in nuclear acoustic resonance (NAR) experiments in the intermediate magnetic field range[1,2] where the energy-level splitting due to the Zeeman effect is approximately equal to the energy-level separation due to the nuclear electric quadrupole interaction. Buttet and Bailey[1] determined at 4.2 K the quadrupole coupling constants, Knight shifts, and linewidths for $^{185,187}$Re, but were unable to determine the dynamic coupling mechanism. Stachel and Bommel[2] studied the temperature dependencies of the $^{185,187}$Re Knight shifts and quadrupole coupling constants between 2 and 150 K.

In this paper we report the first quadrupole resonance experiment in a small magnetic field using NAR on a rhenium metal single crystal. We also report 4.2-K and 77.8-K $^{185,187}$Re nuclear quadrupole coupling constants (magnitude and sign), line-shape studies (line shapes, linewidths, and determination of the square root of the second moments for indirect exchange and a frequency spread of the quadrupole coupling constant), and determination that the dynamic acoustic wave-nuclear spin coupling in rhenium metal is via the dynamic quadrupole interaction. A previous paper[3] did observe the quadrupole spectra in a small magnetic field of $^{121,123}$Sb in antimony metal with the use of a SQUID acoustomagnetic resonance spectrometer. NAR measures an attenuation change while the SQUID acoustomagnetic system measures a magnetization change, both produced by acoustic standing waves at the magnetic-resonance frequency.

Rhenium metal has a close-packed hexagonal structure with the $c$ axis along the [0001] direction. The $^{185}$Re and $^{187}$Re nuclei have nuclear spin $I=\frac{5}{2}$, quadrupole moments of 2.36 and 2.24 b, magnetic dipole moments of 3.1437 and 3.1760 nuclear magnetons, and natural abundances of 37.40% and 62.60%, respectively.

## II. THEORY

Das and Hahn[4] show for an axially symmetric electric-field gradient and for half-integral spins that there are $I+\frac{1}{2}$ doubly degenerate energy levels, $E_m$; a small magnetic field $H$ at an angle $\theta$ with respect to the symmetry axis removes the degeneracy, and the energy levels for $m > \frac{1}{2}$ are

$$E_{\pm m} = A\,[3m^2 - I(I+1)] \mp m\hbar\gamma H\cos\theta\ ,$$

where

$$A = \frac{e^2qQ}{4I(2I-1)}\ ,$$

$eq$ is the $zz$ component of the electric-field gradient tensor, $Q$ is the electric quadrupole moment, and $\gamma$ is the nuclear gyromagnetic ratio. For the original degenerate $m=\frac{1}{2}$ energy level, the presence of a small $H$ leads to $\psi_+$ and $\psi_-$ energy states, which are a mixture of $\psi_{+1/2}$ and $\psi_{-1/2}$ states,

$$E_{\pm} = A\,[\tfrac{3}{4} - I(I+1)] \mp \frac{f}{2}\hbar\gamma H\cos\theta\ ,$$

where

$$f\cos\theta = [\cos^2\theta + (I+\tfrac{1}{2})^2\sin^2\theta]^{1/2}\ , \tag{1a}$$

$$\psi_+ = \psi_{+1/2}\sin\alpha + \psi_{-1/2}\cos\alpha\ , \tag{1b}$$

$$\psi_- = \psi_{-1/2}\sin\alpha - \psi_{+1/2}\cos\alpha\ , \tag{1c}$$

and

$$\tan\alpha = [(f+1)/(f-1)]^{1/2}\ . \tag{1d}$$

For spin $I=\frac{5}{2}$, there are three doubly degenerate energy levels; in the presence of $H$, each degenerate level splits into two levels. The four transitions studied in this research are labeled and shown with arrows in Fig. 1.

 

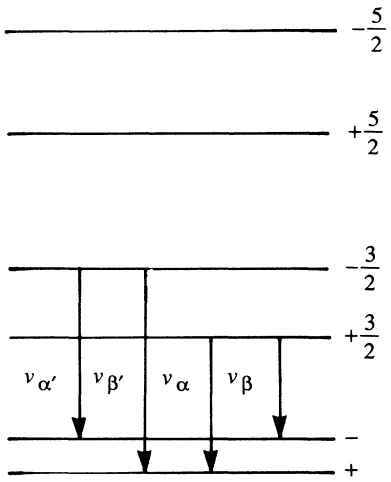


FIG. 1. Arrangement of energy levels for $I=\frac{5}{2}$, an axially symmetric interaction in the presence of a small magnetic field, and positive $A$. The transitions observed are shown with downward arrows.

Frequencies for these transitions are

$$\nu_{\alpha}=\frac{6A}{h}-\frac{3-f}{2}\frac{\gamma}{2\pi}H\cos\theta\ , \tag{2a}$$

$$\nu_{\beta}=\frac{6A}{h}-\frac{3+f}{2}\frac{\gamma}{2\pi}H\cos\theta\ , \tag{2b}$$

$$\nu_{\alpha'}=\frac{6A}{h}+\frac{3-f}{2}\frac{\gamma}{2\pi}H\cos\theta\ , \tag{2c}$$

and

$$\nu_{\beta'}=\frac{6A}{h}+\frac{3+f}{2}\frac{\gamma}{2\pi}H\cos\theta\ . \tag{2d}$$

There are two NAR dynamic coupling mechanisms in nonmagnetic metals[5] which can introduce acoustic energy into a nuclear spin system at the frequency of one of the transitions in Eqs. (2a)–(2d): Alpher-Rubin coupling and quadrupole coupling. Two important signatures of dynamic Alpher-Rubin coupling for shear waves[6] are that the transition probability is proportional to $\cos^4\theta$ when the shear polarization is in the plane of rotation defined by the elastic wave propagation direction and the external magnetic field and to $\cos^2\theta$ when the shear polarization is perpendicular to this plane.

For both dynamic quadrupole coupling and dynamic Alpher-Rubin coupling, dynamic elastic strain $\epsilon_{kl}$ is introduced into the crystal by driving a piezoelectric transducer which is part of the composite resonator consisting of transducer, bond, and rhenium single crystal. Dynamic nuclear electric quadrupole coupling involves a defined $S$ tensor which relates the dynamic electric-field gradient $V_{ij}$ to the dynamic elastic strain

$$V_{ij}=\sum_{kl}S_{ijkl}\epsilon_{kl}\ .$$

For hexagonal close-packed symmetry ($6/mmm$), the nonzero components of the fourth rank polar tensor $S$ can be determined using the methods of Fumi and Ripamonti.[7] One must also use the fact that the $S$ tensor is symmetric in $i$ and $j$ and also in $k$ and $l$. In Voigt notation, the derived $S$ tensor is shown below:

$$\begin{matrix} S_{11} & S_{12} & S_{13} & 0 & 0 & 0 \\ S_{12} & S_{11} & S_{13} & 0 & 0 & 0 \\ S_{31} & S_{31} & S_{33} & 0 & 0 & 0 \\ 0 & 0 & 0 & S_{44} & 0 & 0 \\ 0 & 0 & 0 & 0 & S_{44} & 0 \\ 0 & 0 & 0 & 0 & 0 & \frac{1}{2}(S_{11}-S_{12}) \end{matrix}\ .$$

Note that the $S$ tensor for this crystal symmetry is not symmetric ($S_{13}\neq S_{31}$), a point first discussed by Ströbel and Müller.[8] We choose $x$ to be along the $[11\bar{2}0]$ direction, $y$ along $[\bar{1}100]$, and $z$ along [0001], as shown in Fig. 2. The angle $\theta$ is defined to be the angle in the plane defined by the $[11\bar{2}0]$ and [0001] directions and measured from the [0001] direction to the direction of the external magnetic field $H$. For the particular case of the acoustic shear mode propagation direction along the $z$ direction, the following electric-field gradient elements can be computed following the procedures in Bolef.[9]

$$V_{\zeta[x]\pm1}=\frac{1}{\sqrt{6}}(\cos^2\theta-\sin^2\theta)S_{44}\epsilon_{zx}\ , \tag{3a}$$

$$V_{\zeta[x]\pm2}=-\frac{1}{\sqrt{6}}\sin\theta\cos\theta S_{44}\epsilon_{zx}\ , \tag{3b}$$

$$V_{\zeta[y]\pm1}=\frac{1}{\sqrt{6}}\cos\theta S_{44}\epsilon_{zy}\ , \tag{3c}$$

and

$$V_{\zeta[y]\pm2}=-\frac{1}{\sqrt{6}}\sin\theta S_{44}\epsilon_{zy}\ , \tag{3d}$$

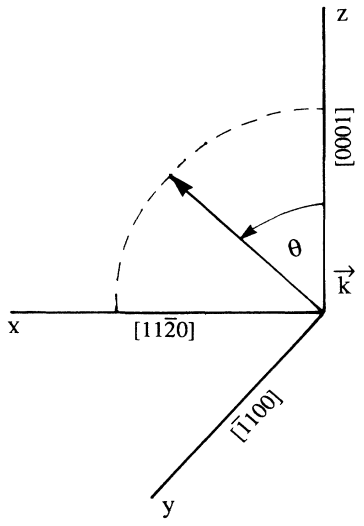


FIG. 2. Definition of $x$, $y$, $z$ and the angle $\theta$ in terms of the hexagonal crystal axes.

where $\zeta$ is the polarization direction of the shear mode. Dynamic quadrupole transition probabilities for $\Delta m = \pm 1$ and $\Delta m = \pm 2$ transitions are given in Eqs. (4a) and (4b), respectively,

$$W_{m,m\pm1} = B\xi^2 V^2_{\zeta\pm1} , \tag{4a}$$

$$W_{m,m\pm2} = B\eta^2 V^2_{\zeta\pm2} , \tag{4b}$$

where $B = (A/\hbar)^2 g(\nu)/4$,

$$\xi^2 = (2m \pm 1)^2 (I \pm m + 1)(I \mp m) ,$$

and

$$\eta^2 = (I \mp m)(I \mp m - 1)(I \pm m + 1)(I \pm m + 2) .$$

For spin $I = \frac{5}{2}$ and transitions between the $\pm\frac{3}{2}$ levels and the $\pm$ mixed levels, $\xi^2 = 32$ and $\eta^2 = 72$. Because dynamic quadrupole coupling allows both $\Delta m = \pm 1$ and $\Delta m = \pm 2$ transitions, all four transitions given in Fig. 1 and whose frequencies are given in Eqs. (2a)–(2d) may have both $\Delta m = \pm 1$ and $\Delta m = \pm 2$ contributions. The amount of each contribution is determined by the angle $\theta$ and the use of Eqs. (1a)–(1d).

The fact that $\psi_+$ and $\psi_-$ are mixed states of $\psi_{1/2}$ and $\psi - 1/2$ and that NAR with dynamic quadrupole coupling can observe both $\Delta m = \pm 1$ and $\Delta m = \pm 2$ transitions, allows NAR to determine the signs of quadrupole coupling constants. For the case of $y$ polarization shear waves and $\theta = 43.3°$, the largest frequency transition [Eq. (2d)] is from $\psi_{-3/2}$ to the $\psi_\pm$ mixed state for a positive $A$ and from the $\psi_{+3/2}$ to the $\psi_-$ mixed state for negative $A$. The dynamic quadrupole coupling transition probability between the $\psi_{-3/2}$ and the $\psi_+$ states involves a cross term which is negative [from the $-$ term in Eq. (3d)] (refer to the Appendix). However, the dynamic quadrupole coupling transition probability between the $\psi_{3/2}$ to the $\psi_-$ states has a cross term which is positive [from the $-$ terms in Eq. (1c) and Eq. (3d)]. Therefore, by computing the ratio of the measured transition probability for $\theta = 0°$ and $\theta = 43.3°$, it is possible to determine the sign of $A$.

## III. EXPERIMENTAL

A single crystal of rhenium 99.99% pure was purchased from Aremco Products. The rhenium crystal, approximately 0.5 in. diameter by 0.5 in. long, was oriented and ground with a set of parallel faces whose perpendicular is within $\pm 1°$ of the [0001] direction. Scratches along the sides of the crystal indicate the $[\bar{1}100]$ direction to within $\pm 1°$. A composite resonator was constructed using a 0.375-in. diameter, quartz, 12.5-MHz AT cut transducer, Nonaq grease bond, and the rhenium crystal. The transducer polarization direction was chosen along the $x$ or $y$ direction and the propagation direction was along the $z$ direction. For both polarizations, the plane of rotation of the magnetic field was the plane which includes the $[11\bar{2}0]$ and [0001] directions, as shown in Fig. 2. The composite resonator was mounted in a low-temperature probe. A 50-$\Omega$ probe transmission line connected the composite resonator to the sample arm of a commercial hybrid junction which is the bridge element of a computer-controlled ultrasonic reflection bridge spectrometer.[10] Müller[11] discusses the general properties of reflection bridge spectrometers used in NAR.

From the quadrupole coupling constants measured by the previous NAR experiments on rhenium metal,[1,2] the expected zero magnetic-field quadrupole transition from $\frac{3}{2}$ to $\frac{1}{2}$ level is approximately 38.38 MHz for $^{187}$Re and 40.65 MHz for $^{185}$Re. The transducer was driven at its third harmonic response. At temperatures $< 180$ K, the Nonaq bond is rigid and the composite resonator response consists of mechanical standing-wave resonances spread in frequency from 35 to over 41 MHz. Typical mechanical resonances near the center of the third harmonic response at 77.8 K have frequency widths of 2 kHz and the real part of the composite resonator impedance at the mechanical resonance center is approximately 800 $\Omega$. The low-temperature probe was placed in a Varian electromagnet with Field-Dial (Hall probe) magnetic-field regulation and control; the magnet could be rotated about a vertical axis. The Field-Dial system, magnetic-field sweep system, and modulation field amplitude were calibrated at 300 K using the $^1$H NMR in a doped water system for magnetic fields from 500 to 1200 G.

The condition for quadrupole resonance in a small field was determined by choosing a mechanical resonance center at the appropriate frequency for a particular angle $\theta$ so that the magnetic-field center could be chosen to meet one of the four transitions shown in Fig. 1 but still be a small field $[(\gamma/2\pi)H \ll e^2qQ/h]$. In order to measure the resonance, the magnetic field was swept about the center field and magnetic-field modulation was used at 37 Hz with an amplitude of 17 or 34 G. Phase-sensitive detection was used at 37 Hz with a 1.25-s time constant and the first derivative absorption and dispersion resonance signals were digitized and averaged. Typical magnetic-field sweeps times were 300 s and the sweep ranges were 250 or 500 G for the very broad $\frac{3}{2}$ to $\frac{1}{2}$ transitions. rf detection was done with phase-sensitive detection so that both the absorption and dispersion signals could be studied and so that signal averaging would be effective with one-pass signal to noise ratios less than 0.2.[12] By adjusting the frequency to the center of a mechanical resonance and then tuning a phase shifter in the rf phase-sensitive detection arm of the spectrometer for the "in-phase" or "out-of-phase" mechanical resonance responses,[13] it is possible to choose either the NAR absorption or dispersion response.

NAR quadrupole resonance signal amplitudes are dependent on frequency, magnet angle, numerical factors in the NAR transition probability, temperature, natural abundance of the nuclear spin system, acoustic power level, bond properties of the composite resonator, magnetic-field modulation amplitude, and skin depth for the modulation field. The best $^{187}$Re NAR first derivative of the dispersion signal to noise ratio was 0.3 for a single pass at 77.8 K and $\theta = 90°$ with the conditions described above. At 4.2 K, the signal to noise increased by a factor of 6 over the 77.8 K value. However, the 4.2-K resonances were seen under conditions of saturation, the Re

skin depth prevented complete penetration of the 37-Hz modulation field, and the resonance sweep baselines were altered by the dc Alpher-Rubin[14] effect. Therefore most data were taken at 77.8 K. The electrical power applied to the composite resonator was kept approximately at the value 3.24 $\mu$W, which is a power level that did not show the effects of saturation at 77.8 K.

The direction of $[11\bar{2}0]$ was determined experimentally from study of the $^{187}$Re NAR signal at a magnet angle near $\theta=90°$. At $\theta=90°$, the $+\frac{3}{2}$ and $-\frac{3}{2}$ energy levels coincide and the equal frequencies $\nu_{\beta'}$ and $\nu_\alpha$ produce $\Delta m=\pm 2$ NAR signals centered at the same resonance magnetic field. If $\theta=89°$ or 91°, the $+\frac{3}{2}$ and $-\frac{3}{2}$ levels are split and the frequencies $\nu_{\beta'}$ and $\nu_\alpha$ are not equal; the observed NAR signal mainly consists of two $\Delta m=\pm 2$ transitions separated by 50 G at a field of 1000 G. The effective NAR linewidth change with a small change in $\theta$ is so large that the $[11\bar{2}0]$ direction can be determined within $\pm\frac{1}{2}°$.

## IV. EXPERIMENTAL RESULTS

### A. Dynamic coupling

The $^{185,187}$Re NAR quadrupole resonance first derivatives of the dispersion signals were observed at the magnetic field angles ($\theta$) of 0°, 43.3°, and 90° and at 77.8 and 4.2 K with both polarization directions of the shear transducer given by the strains in Eqs. (3a)–(3d). For $\theta=0°$, $f=1$, $\alpha=90°$, and $\psi_+=\psi_{1/2}$, and $\psi_-=\psi_{-1/2}$. Therefore, $\nu_\alpha$ and $\nu_{\alpha'}$ are $\pm 1$ transitions and $\nu_\beta$ and $\nu_{\beta'}$ are $\pm 2$ transitions. The $\Delta m=\pm 1$ transitions $\nu_\alpha$ and $\nu_{\alpha'}$ are observed; however, the $\Delta m=\pm 2$ transitions $\nu_\beta$ and $\nu_{\beta'}$ are not seen. This is exactly what the dynamic quadrupole transition probabilities of Eqs. (4a) and (4b) and the transition probabilities of dynamic Alpher-Rubin coupling predict.

For $\theta=90°$, $\alpha=45°$, the $\pm$ levels are mixed with equal amounts of $\psi_{+1/2}$ and $\psi_{-1/2}$, and the $\pm 3/2$ levels coincide. The dynamic quadrupole coupling field gradient element in Eq. (3c) and the dynamic Alpher-Rubin transition probability angular dependences predict that there should be no $\Delta m=\pm 1$ transitions. However, $\Delta m=\pm 2$ transitions are allowed by the dynamic quadrupole coupling, Eq. (3d), and a resonance which is narrower than that observed at $\theta=0°$ is found. From the observation of a $\Delta m=\pm 2$ transition at 90° and not at 0° and a $\Delta m=\pm 1$ transition at 0° and not at 90°, we conclude that the coupling is dynamic quadrupole coupling.

### B. Quadrupole coupling constant

From the known frequency, magnetic field, magnet angle, and temperature, the quadrupole coupling constants for $^{185,187}$Re at 4.2 and 77.8 K are given in Table I. The precision of these measured quadrupole coupling constants is limited by the large width of the resonances and the 10/1 signal-to-noise ratio attainable in 48 h of signal averaging. Because the resonance line-shape tails exceeded the sweep window of 500 G at $\theta=0°$, the dispersion signal was used in all cases for quadrupole coupling constant determination. The first derivative of the dispersion signal (the observed signal with audio phase-sensitive detection) is a symmetric resonance structure, as shown in Fig. 3 for $^{185}$Re at 77.8 and at $\theta=90°$. With careful tuning of the rf phase shifter, it is possible to obtain a dispersion signal with symmetric baselines and centered in the magnetic-field sweep window.

TABLE I. Magnitudes of the measured nuclear electric quadrupole coupling constants for $^{185}$Re and $^{187}$Re.

| Temperature (K) | Nucleus | $e^2qQ/h$ (MHz) |
|---|---|---|
| 77.8 | $^{187}$Re | 255.920±0.013 |
| 77.8 | $^{185}$Re | 270.966±0.013 |
| 4.2 | $^{187}$Re | 255.478±0.013 |
| 4.2 | $^{185}$Re | 270.430±0.013 |

The sign of the quadrupole coupling constant can be determined from the measured ratio of the transition probabilities at $\theta=0°$ and $\theta=43.3°$. At $\theta=43.3°$, $f=3$ and $\nu_\alpha=\nu_\beta$ and these transitions do not depend on $H$. We compare the $\nu'_\alpha$ transition at 0° with the $\nu'_\beta$ transition at 43.3°. Dynamic quadrupole coupling transition probability predicted ratios are 5.67, if $A$ is positive, and 0.63 if $A$ is negative. The experimental ratio of the $\theta=0°$ to the $\theta=43.3°$ peak-to-peak amplitudes of the first derivative of the absorption signal is 2.3±0.2, when the same modulation amplitude is used; however, the ratio of the $\theta=0°$ to the $\theta=43.3°$ peak-to-peak linewidths is 1.6±0.1. The experimental transition probability ratio is proportional to the ratio of the amplitudes times the ratio of the square of the linewidths, for a constant modulation field with different linewidths. Therefore, the measured transition probability ratio $\theta=0°$ to $\theta=43.3°$ is

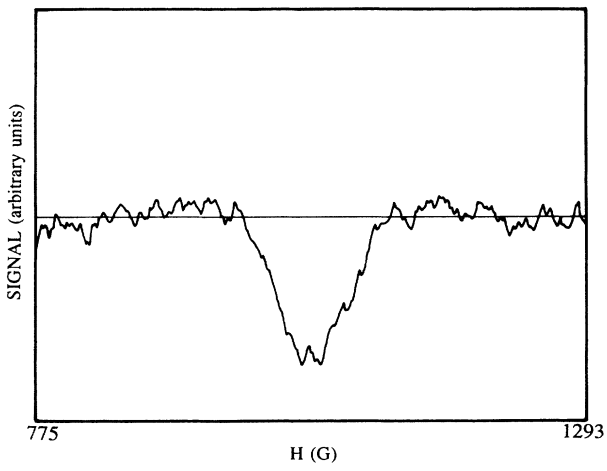


FIG. 3. $^{185}$Re NAR $\Delta m=\pm 2$ $\nu_\beta$ transition first derivative dispersion signal at $\theta=90°$, 48-h signal averaging, 77.8 K, 500-G sweep in 5 min, 1.25-s time constant, 34-G amplitude modulation at 37 Hz, and 39.117 400 MHz.

$2.3\times(1.6)^2=5.9\pm0.4$ and we conclude that $A$ is positive. This determination of the coupling constant being positive is in disagreement with a nuclear specific-heat determination of $A$ being negative.[15]

### C. Resonance line shapes and linewidths

The $^{187}$Re and $^{185}$Re NAR line shapes and linewidths are the same. A first derivative of a Gaussian line shape can be fit to the experimental first derivative of the absorption $^{187}$Re line shape as shown in Fig. 4. Because of the low (10/1) signal-to-noise ratio after 48 h of signal averaging, we have fit the first derivative of a Gaussian line shape to the absorption first derivative in all that follows.

At 77.8 K and $\theta=90°$, the $^{187}$Re $\Delta m=\pm2$ first derivative of the absorption, peak-to-peak linewidth is $73\pm4$ G with either a 17-G or 34-G amplitude modulation field; the 34-G amplitude was used in order to obtain the largest possible signal-to-noise ratio. At $\theta=0°$, the $^{187}$Re $\Delta m=\pm1$ first derivative of the absorption line-shape peak-to-peak width is $98\pm4$ G. At $\theta=43.3°$, the first derivative of the $\Delta m=\pm1$ absorption line-shape peak has a width of $68\pm4$ G. These linewidths are independent of magnetic field over the range investigated, from 200 to 1200 G. Since the line shapes are Gaussian shapes within the signal-to-noise ratio, it is possible to compute their second moments $S_2$. We find the second moments are at $\theta=0°$, $S_2=2400$ G$^2$, at $\theta=43.3°$, $S_2=1150$ G$^2$, and at $\theta=90°$, $S_2=1350$ G$^2$. In a nonmagnetic single-crystal conductor, the line-broadening mechanisms,[16] which vary with the direction of the external field, are direct dipole-dipole, pseudodipolar, and quadrupole broadening. An isotropic indirect exchange broadening[16] is also present in large $Z$ atoms.

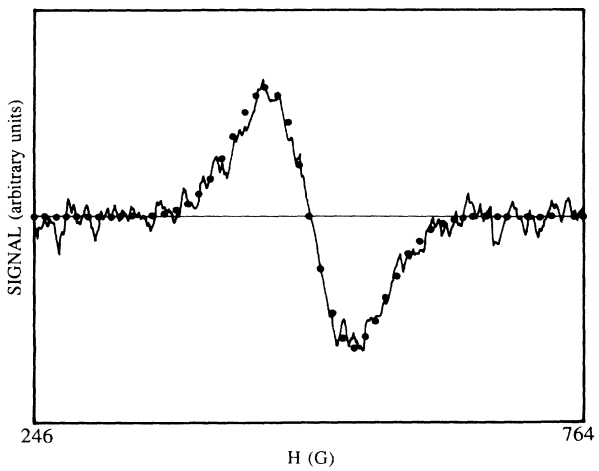


FIG. 4. $^{187}$Re NAR $\Delta m=\pm2$ $\nu_\beta$ transition first derivative absorption signal at $\theta=90°$, 48-h signal averaging, 77.8 K, 500-G sweep in 5 min, 1.25-s time constant, 34-G amplitude modulation at 37 Hz, and 39.117 400 MHz. The circles are a theoretical Gaussian first derivative plotted using the experimental peak-to-peak width, peak-to-peak amplitude, and center position.

By using the ratio of the second moments determined from experiment at two different angles and comparing these with the theoretical ratios for direct dipole-dipole, pseudodipolar, and quadrupole interactions, it is possible to show that another interaction must be present.

An expression for the dipole-dipole second moment in a hexagonal crystal has been given by Löshe[17] and is shown in Eqs. (5) and (6);

$$\langle\Delta\nu^2\rangle=\frac{3}{8}\frac{\gamma^4}{(2\pi)^4}h^2[I(I+1)](m+n\cos^2\theta+o\cos^4\theta)\,, \tag{5}$$

where

$$m=\tfrac{1}{4}\sum_k r_{jk}^{-6}(11-30\zeta^2+27\zeta^4)\,, \tag{6a}$$

$$n=\tfrac{1}{2}\sum_k r_{jk}^{-6}(-15+126\zeta^2-135\zeta^4)\,, \tag{6b}$$

$$o=\tfrac{1}{4}\sum_k r_{jk}^{-6}(27-270\zeta^2+315\zeta^4)\,, \tag{6c}$$

$r_{jk}$ is the position vector from the $j$ to the $k$ nuclear positions, and $\zeta$ is the direction cosine of the angle defined by $r_{jk}$ and the [0001] direction. The sums of $m$, $n$, and $o$ have been evaluated out to the 28th shell from a reference nuclear position and, in units of $a^{-6}$, where the hexagonal Re lattice constant $a=0.619\,26c=2.7608$ Å, are $m=24.36$, $n=-12.13$, $o=13.71$. The largest dipole-dipole second moment is when $\theta=0°$. With the assumption of a Gaussian line shape, the expected dipole-dipole peak-to-peak linewidth is 5.0 G. Since the observed peak-to-peak widths are ten times larger, the dominant broadening is not dipole-dipole broadening.

Bloembergen and Rowland[18] define the pseudodipolar interaction constant $B_{jk}$ so that the dependence on $r_{jk}$ is in the constant. $B_{jk}$ is expected to fall off[16] at large distances as $r_{jk}^{-3}$, but its exact distance dependence is not known. The ratio of the distances from a reference nuclear position to the first two shells is 0.992 587. The lattice sums $m$, $n$, and $o$ for the first two shells are $m=21.16$, $n=-15.93$, and $o=18.94$. By using these values in Eq. (5), one can compute quantities proportional to the second moments for pseudodipolar coupling for the first two neighbor shells and compare the ratio at $\theta=0°$ to $\theta=90°$ and at $\theta=0°$ to $\theta=43.3°$ of these quantities with the ratio of the second moments found from the experimental line shapes. Such comparison of ratios shows disagreement with the experimental second moment ratios for both those computed with the pseudodipolar interaction and those with the direct dipole-dipole interaction. The presence of the pseudodipolar interaction alone with the smaller dipole-dipole interaction cannot explain the observed experimental linewidth anisotropy and there must be another line-broadening mechanism present.

A possible source of an electric-field gradient that could produce the observed anisotropy in the observed linewidths is a spread in the value of the nuclear electric quadrupole coupling constant due to crystal imperfec-

tion. In this case, the electric-field gradient would be along the [0001] direction and the line broadening would be proportional to $(3\cos^2\theta-1)$. At $\theta=54.75°$, this expression is zero and the linewidth should reduce to the direct dipole-dipole width of 5.0 G if only the direct dipole-dipole and quadrupole broadenings were present. At $\theta=54.7°$, the experimental absorption first derivative peak-to-peak value is the 75–80-G range.

We conclude in addition to direct dipole-dipole broadening that we have indirect exchange present with possible pseudodipolar and/or quadrupolar broadening mechanisms. In order to determine which of the above broadening mechanisms are present, we write the experimental second moment $S_2$ as the sum of second moments due to indirect exchange, $C^2$, and to the nuclear electric quadrupole, $D^2$

$$S_2=C^2+D^2(3\cos^2\theta-1)^2$$

and compute $C$ and $D$ at $\theta=0°$, 43.3°, and 90°. The values of $C$ and $D$ that are consistent for all three angles are $C=32\pm2$ G and $D=19\pm2$ G. A similar computation using the sum of indirect exchange second moment and pseudodipolar second moment or pseudodipolar and nuclear electric quadrupole second moments at the three angles gives inconsistent results. We finally conclude that the dominant broadening mechanisms are indirect exchange and nuclear electric quadrupole with values of $C$ and $D$ given above. The spread in the nuclear electric quadrupole coupling constant value is $18\pm2$ kHz. Validity of the above analysis is because of the inequalities

$$\frac{\gamma_{187}}{2\pi}H=979\,040>C=32\,300>\frac{\gamma_{187}-\gamma_{185}}{2\pi}H=9800>\frac{\gamma_{187}}{2\pi}\delta H_{pp\ \text{dipole-dipole}}=5000\ ,$$

where the numbers are in Hz and the field $H$ is 1000 G.

## V. SUMMARY

It has been shown that NAR is a very effective technique for magnetic-resonance studies of quadrupole spectra in a very small magnetic field and for axial symmetry. Not only can the electric quadrupole coupling constant magnitude be determined, but also its sign, when transitions from the $\pm\frac{3}{2}$ to the $\pm$ mixed levels are studied. The coupling mechanism between dynamic elastic strain and the nuclear spin systems has been shown to be the dynamic quadrupole interaction; however, the Alpher-Rubin interaction does effect the ultrasonic velocity and attenuation of the composite resonator. Because each transition is, in general, the sum of both $\Delta m=\pm1$ and $\pm2$ contributions, the magnetic resonance can be studied as a function of angle for all angles. In this paper, the angular dependence of the magnetic resonance linewidth has shown the presence of the indirect exchange and static nuclear electric quadrupole interactions and allowed a determination of a spread in the quadrupole coupling constant. Finally, the use of a NAR bridge spectrometer brings high-sensitivity measurements to nuclear electric quadrupole resonance in a small field at frequencies above 5 MHz.

## ACKNOWLEDGMENTS

The author thanks Professor Emeritus Dan I. Bolef and Professor Peter A. Fedders for many useful discussions regarding the research.

## APPENDIX A: TRANSITION PROBABILITY CROSS TERMS

The transition probability from $\psi_{-3/2}$ to $\psi_+$ for $\epsilon_{zy}$ strain is

$$\begin{aligned}W_{-3/2,+}&=\frac{1}{4\hbar^2}|(\psi_{-3/2}|H|\psi_+)|^2g(\nu)\\&=\frac{g(\nu)}{4\hbar^2}[\,|(\psi_{-3/2}|H|\psi_{1/2}\sin\alpha)|^2+|(\psi_{-3/2}|H|\psi_{-1/2}\cos\alpha)|^2+2(\psi_{-3/2}|H|\psi_{1/2}\sin\alpha)(\psi_{-3/2}|H|\psi_{-1/2}\cos\alpha)]\\&=\frac{B\epsilon_{zy}^2g(\nu)S_{44}^2}{6}(\eta^2\sin^2\alpha\sin^2\theta+\xi^2\cos^2\alpha\cos^2\theta-2\eta\xi\sin\alpha\sin\theta\cos\alpha\cos\theta)\ .\end{aligned}$$

The transition probability from $\psi_{+3/2}$ to $\psi_-$ has identical terms with the equation above except that the cross term has an additional multiplicative $-1$ term from $\psi_-$.

[1]J. Buttet and Philip K. Bailey, Phys. Rev. Lett. **24**, 1220 (1970).
[2]M. Stachel and H. E. Bömmel, Appl. Phys. **A30**, 27 (1983).
[3]K. S. Pickens, D. I. Bolef, M. R. Holland, and R. K. Sundfors, Phys. Rev. B **30**, 3644 (1984).
[4]T. P. Das and E. L. Hahn, in *Solid State Physics*, edited by Frederick Seitz and David Turnbull (Academic, New York, 1958), Suppl. 1, Nuclear Quadrupole Resonance Spectroscopy.
[5]R. K. Sundfors, D. I. Bolef, and P. A. Fedders, Hyperfine Interact. **14**, 271 (1983).
[6]Peter A. Fedders, Phys. Rev. B **7**, 1739 (1973).
[7]F. G. Fumi and C. Ripamonti, Acta Crystallogr. **A36**, 535

(1980); **A36**, 551 (1980).
[8]Bernard Ströbel and Volker Müller, Phys. Rev. B **24**, 6292 (1981).
[9]D. I. Bolef, in *Physical Acoustics,* edited by W. P. Mason (Academic, New York, 1966), Vol. 4A, Chap. 3.
[10]R. K. Sundfors, Rev. Sci. Instrum. (to be published).
[11]V. Müller, J. Phys. E **8**, 1 (1975).
[12]E. O. Stejskal, Rev. Sci. Instrum. **34**, 971 (1963).
[13]D. I. Bolef and J. G. Miller, in *Physical Acoustics,* edited by W. P. Mason and R. N. Thurston (Academic, New York, 1971), Vol. 8, Chap. 3.
[14]R. A. Alpher and R. J. Rubin, J. Acoust. Soc. Am. **26**, 452 (1954).
[15]P. E. Gregers-Hansen, M. Krusius, and G. R. Pickett, Phys. Rev. Lett. **27**, 38 (1971).
[16]C. P. Slichter, *Principles of Magnetic Resonance* (Springer-Verlag, New York, 1980).
[17]A. Löshe, *Kerninduktion* (VEB Deutsher Verlag der Wissenschaften, Berlin, 1957).
[18]N. Bloembergen and T. J. Rowland, Phys. Rev. **97**, 1679 (1955).